Journal of Computational Physics 342 (2017) 253–266

Contents lists available at ScienceDirect

Journal of Computational Physics

www.elsevier.com/locate/jcp

An efficient two-step Monte Carlo method for heat conduction in nanostructures

Yu-Chao Hua (华钰超), Bing-Yang Cao (曹炳阳) *

Key Laboratory for Thermal Science and Power Engineering of Ministry of Education, Department of Engineering Mechanics, Tsinghua University, Beijing 100084, China

ARTICLE INFO

Article history:
Received 1 July 2016
Received in revised form 6 April 2017
Accepted 13 April 2017
Available online 20 April 2017

Keywords:
Phonon Monte Carlo
Heat conduction
Nanostructure
Effective thermal conductivity

ABSTRACT

Research on the heat conduction in nanostructures has drawn much attention due to their potential applications in thermoelectric devices. Although the phonon tracing Monte Carlo (MC) technique, where the trajectories of individual phonons are simulated independently, has been extensively used for simulating the heat conduction in nanomaterials, it cannot efficiently simulate the phonon transport in the large area periodic nanostructures yet, due to the demand of absorbing boundaries. In the present work, we develop a two-step phonon tracing MC method to solve this problem. At the first step, the initial phonon transmittance and the phonon emission distributions at the internal virtual boundary are obtained by simulating phonon transport in the initial simulation unit that is directly in contact with the phonon bath. At the second step, the internal phonon transmittance is calculated for the internal simulation units according to the internal boundary phonon emission distributions. Since the whole structure can be simplified as a one-dimensional phonon transport system, the total phonon transmittance can be readily calculated via the combination of initial and internal phonon transmittances, and the effective thermal conductivity is then derived. Furthermore, for verification, we calculate the effective thermal conductivities of three typical nanostructures, that is, the cross-plane and in-plane nanofilms and the periodic nanoporous structures, by using the theoretical models, the standard and the two-step MC simulations, respectively. The two-step MC method well predicts the results calculated by the standard MC simulations and the theoretical models. More importantly, the computation time of the two-step MC simulation is at least one order of magnitude less than that of the standard MC simulation, while its under-prediction can be less than 10% even 5%.

1. Introduction

Periodic semiconductor nanostructures, such as phononic crystals, have shown great potentials for developing the highly-efficient thermoelectric devices [1–3]. Researchers demonstrated that by etching periodic nanoscale holes in silicon thin films (i.e. phononic crystals) the effective thermal conductivity is significantly reduced due to the phonon-boundary scattering, while only a minor effect occurs on their electrical properties, and thus the dimensionless figure of merit (ZT) can be improved. Therefore, the study on the heat conduction in the periodic semiconductor nanostructures has been necessarily

* Corresponding author.
E-mail address: caoby@mail.tsinghua.edu.cn (B.-Y. Cao).

http://dx.doi.org/10.1016/j.jcp.2017.04.042
0021-9991/

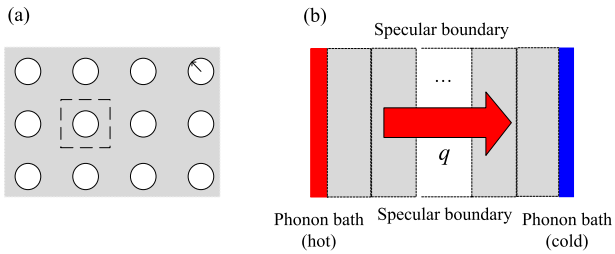

Fig. 1. (a) Schematic for a typical large area periodic nanostructure: phononic crystals. (b) A temperature difference is applied in the nanostructure to induce a heat flow, and then the effective thermal conductivity can be calculated by using Fourier's law.

essential for the further development of the new-generation thermoelectric materials [4–6]. Phonons predominate the thermal transport in semiconductors [7]. In nanostructures whose characteristic lengths are comparable to the phonon mean free path (MFP), ballistic transport and boundary scattering will make the effective thermal conductivity dependent on the geometry and size, indicating a violation of the classical Fourier's law [8].

Generally, the phonon Boltzmann transport equation (BTE) is employed to characterize the thermal transport in nanostructures [9,10]. Monte Carlo (MC) simulation has been proven to be a favorable method to solve the phonon BTE [11–31]. Two typical kinds of MC methods are often used to simulate phonon transport in nanostructures: the ensemble MC and the phonon tracing MC. In the ensemble MC simulations, the trajectories of all phonons are simulated simultaneously at each time step [12–18]. Peterson [12] first simulated phonon heat conduction by using this method on the basis of Debye approximation. Afterwards, the ensemble MC method was also employed to study the effective thermal conductivity of nanostructures including nanoporous silicon [14–16], and composites [17,18], etc. In contrast, the phonon tracing MC method simulates the trajectories of individual phonons independently, resulting in a significant reduction of computational expense [11,19–31]. Early in 1989, Klitsner et al. [11] used the phonon tracing MC simulation to study the ballistic heat conduction in the silicon crystals at an extremely-low temperature, neglecting the influence of internal phonon scattering. Then, this method was extended to simulate the phonon transport at room temperature, where the internal phonon scattering becomes significant. Péraud et al. [19] simulated the heat conduction for the transient thermo-reflectance experiment, demonstrating the validity of the phonon tracing method. According to the work of Schleeh et al. [20], this method can also be an efficient technique to investigate the thermal transport in electronics. Besides, Hua et al. [21–25], Ravichandran et al. [26] and Lee et al. [27] employed this method to study the thermal properties of the various nanostructures, including nanofilms, nanowires and nanoporous materials, and the MC simulations could well predict the results obtained by the theoretical models and the experiments. The phonon tracing MC method was also employed to investigate the ultrafast thermal transport process in nanostructures, where the ballistic-diffusive mechanism could be coupled with the heat wave effect [28–31]. To be summarized, the phonon tracing method can well handle the problems with complicated geometries and multiple scattering events, and the ultrafast transport processes. When compared to the molecular dynamics (MD) simulation which has been another important simulation technique [32], the phonon tracing MC method holds a considerably less computational expense, and thus it could be employed to study the problems with larger size. Actually, the MD simulation could contain more physical details; for example, in the conventional MC simulations, the boundaries are frequently regarded as rigid, while the MD simulations could better characterize the complexity resulted from the structural relaxation on the edge region [33].

Fig. 1(a) illustrates a typical large area periodic nanostructure. As shown in Fig. 1(b), in MC simulations a temperature difference is usually imposed in the structure to induce a heat flux, and then the effective thermal conductivity can be obtained by using Fourier's law, $k_{\text{eff}} = qL/\Delta T$, where q is the heat flux, L is the distance between these two phonon baths, and ΔT is the temperature difference. Isothermal boundary conditions [13] are frequently applied to establish the temperature difference in the MC simulations, which requires a computational domain consisting of many periods to eliminate the end effects [14–16]. In this case, the exact effective thermal conductivity can be obtained only if the simulation results will no longer vary with further increasing the number of periods, resulting in a considerable large computational expense. Jean et al. [15] investigated the effective thermal conductivity of nanoporous silicon and germanium by using the ensemble MC simulations where the traditional isothermal boundary conditions were used. Wolf et al. [16] also discussed the effects of porosity and roughness on the effective thermal conductivity of silicon nanomesh via the ensemble MC method with isothermal boundary conditions. In order to reduce the computational expense, researchers [14,17] have devoted to developing the periodic boundary conditions to obtain the exact effective thermal conductivity of the large area periodic nanostructures by simulating the phonon transport only in one or several repeating units. A periodic boundary condition specially for the ensemble MC simulation was proposed by Jeng et al. [17] in the simulations of the heat conduction in nanoparticle composites. Then, Hao et al. [14] and Péraud et al. [18] studied the thermal transport in periodic nanostructures following the method proposed by Jeng et al. [17]. As for the phonon tracing MC simulation, the periodic boundary condition could become inapplicable due to the demand of absorbing boundaries [19]. Thus, when using the phonon tracing MC simulation to calculate the thermal conductivity of the phononic crystal nanostructures, Nomura et al. [34] had to choose the distance between phonon baths to be sufficiently large to obtain an exact value. In order to overcome the absence of absorbing boundary when the periodic boundary condition is used in the phonon tracing MC simulations, Péraud et al. [19] suggested

that the phonon tracing could be terminated after several scattering events, but it is still difficult to determine the number of scattering events a phonon must undergo before its tracing can be terminated. In practice, due to the significant computational merit of the phonon tracing MC simulation, it has been extensively used to investigate the phonon transport in nanostructures, but yet even now cannot efficiently handle the problems in the large area periodic nanostructures because of the inapplicability of periodic boundary condition. Therefore, it could be needed to further develop the phonon tracing MC method for the efficient simulation of the heat conduction in the large area periodic nanostructures.

In the present work, a two-step phonon tracing MC method that overcomes the deficiency of the periodic boundary condition is developed to simulate the heat conduction in nanostructures. It contains two basic simulation steps, and can greatly reduce the computation time without destroying the accuracy. Additionally, the numerical experiments for the cross-plane and in-plane nanofilms, and the periodic nanoporous structures, are conducted to verify the two-step MC method.

2. Phonon tracing MC simulation

The phonon tracing MC simulation is based on the phonon BTE [9,10],

$$\vec{v}_g \cdot \nabla f = \frac{f_0 - f}{\tau}, \tag{1}$$

where $\vec{v}_g(\omega)$ is the group velocity, $f = f(\vec{r}, \omega, \varphi, \theta, T)$ is the phonon distribution function, f_0 is the equilibrium distribution function, $f_0 = f_{BE}/4\pi$, and $\tau(\omega, p, T)$ is the relaxation time (ω, φ, θ, T, $\hbar$, k_B, p, and f_{BE} referring to the angular frequency, the azimuthal angle, the polar angle, the temperature, the Dirac constant, the Boltzmann constant, the polarization, and Bose–Einstein distribution, respectively). In MC simulations, phonons are treated as particles, and their motion is simulated by random number sampling, equivalent to directly solving Eq. (1).

In practice, what we simulate is the prescribed phonon bundles but not actual phonons. The intensity of each phonon bundle is defined as, $W = E/N$, where E is the emission phonon energy per area per unit time from the boundary, and N is the number of phonon bundles that we trace in MC simulations. The emitting phonon energy, E, is dependent on the boundary temperature [35,36],

$$E = \sum_p \int_0^{\omega_{\max,p}} v_g(\omega) C_\omega d\omega \frac{T_B}{4}, \tag{2}$$

in which $C_\omega = \hbar\omega \partial f_{BE}/\partial T \mathrm{DOS}(\omega)$, $\mathrm{DOS}(\omega)$ is the phonon density of states, and T_B refers to the boundary temperature. N must be large enough to preserve the simulation accuracy, and energy conservation is guaranteed by conserving the total number of phonon bundles.

The position vector of phonon bundle is defined as $\vec{r} = [x, y, z]$, and the directional vector is $\vec{s} = [\cos(\theta), \sin(\theta)\cos(\varphi), \sin(\theta)\sin(\varphi)]$, where θ is the polar angle and φ is the azimuthal angle. Besides, phonon properties, including dispersion relations and relaxation time, which can be obtained from the first principle method [37] and some empirical models [38], should be input for initialization. It is noted that the gray approximation which assumes phonon properties are frequency-independent, is often adopted. In this case, phonons travel with one average group velocity and the scattering rate is characterized by an average phonon MFP [12,35].

Here, the two most common boundary conditions, i.e., isothermal and adiabatic boundaries, are discussed. An isothermal boundary holds two functions: First, it emits phonons into the computational domain; Second, it also serves as an absorbing boundary to ensure energy conservation. When a phonon bundle emits from an isothermal boundary, its intensity is given in terms of the boundary temperature, and the boundary phonon emission distributions, including angular and spatial distributions, should be obtained according to the properties of boundary. In principle, an isothermal boundary is usually set as phonon black-body [13] in analogy to the black-body wall in photon transport, that is, phonons arriving at it will be completely absorbed. In contrast, for adiabatic boundary, all phonons that strike it will be reflected back into the computational domain. A specular parameter, P, is introduced to describe the possibility of phonon specular scattering at such boundaries. It can be expressed as $P = \exp(-16\pi^2\Delta^2/\lambda^2)$ [7], in which Δ is the root-mean-square value of the roughness fluctuations and λ is phonon wavelength. When P is equal to 1, the phonon scattering is completely specular, and we then have

$$\vec{s}_r = \vec{s}_i + 2|\vec{s}_i \cdot \vec{n}|\vec{n}, \tag{3}$$

in which $\vec{s}_i$ is the incident direction vector, $\vec{s}_r$ is the reflect direction vector, and $\vec{n}$ is the unit surface normal vector. While $P = 0$ corresponds to the diffusive scattering, and the reflecting direction vector should be regenerated.

Fig. 2 illustrates the phonon tracing algorithm of the phonon tracing MC method. Basically, we divide this process to six procedures:

(1) **Initialization**: Input phonon properties, and set the total number of phonon bundles.
(2) **Phonon bundle emission**: Draw the initial properties of a phonon bundle according to the nature of the emitting boundary. These properties, including position $\vec{r}_0 = [x_0, y_0, z_0]$, traveling direction $\vec{s}$, polarization p, angular frequency ω, etc., are determined by random number sampling.

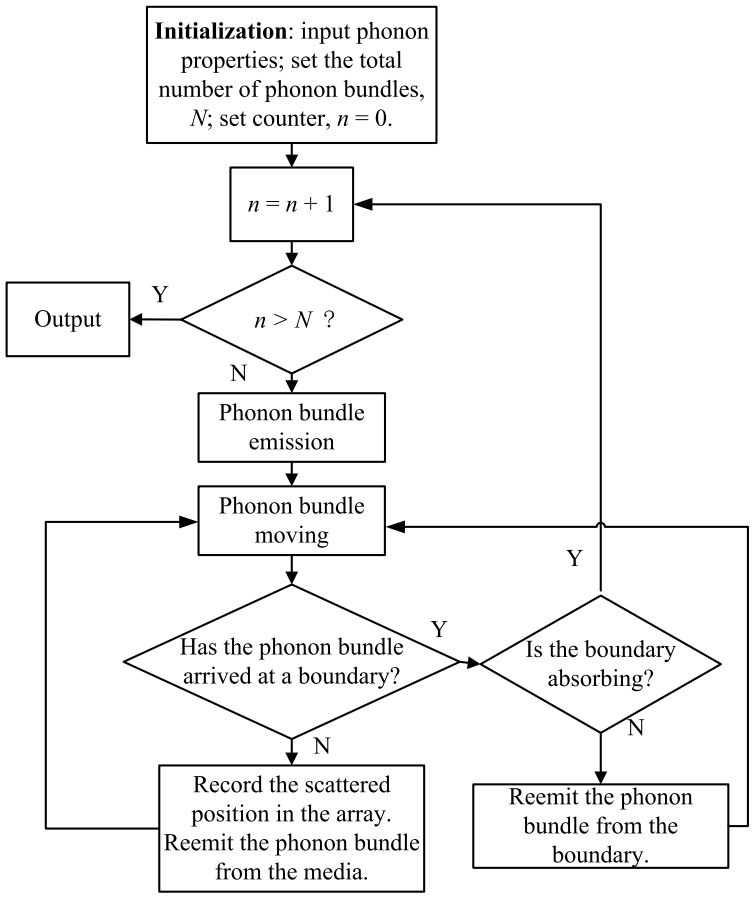

Fig. 2. Phonon tracing algorithm schematic for phonon tracing Monte Carlo simulation.

(3) **Phonon bundle moving**: Calculate the traveling length Δr until the first scattering event and renew the position of phonons, $\vec{r}_{new} = \vec{r}_0 + \Delta r\vec{s}$.
(4) **Boundary scattering**: When a phonon bundle collides with a boundary at $\vec{r}_B$, set $\vec{r}_{new} = \vec{r}_B$. If the boundary is non-absorbing, the phonon bundle should be reflected back into the domain. Then, a random number is drawn. If this random number is less than the specular parameter P, the boundary scattering is specular; otherwise, the boundary scattering is diffusive.
(5) **Phonon bundle reemission**: If a phonon bundle does not collide with boundaries, the phonon should reemit at r_{new}. Then, we set $\vec{r}_0 = \vec{r}_{new}$ and proceed to (3).
(6) **Phonon bundle tracing termination**: If the phonon bundle arrives at the absorbing boundary, the tracing process of this phonon bundle is finished. We then proceed to (2) and begin the tracing of the next phonon bundle.

In the case of small temperature difference, the phonon properties (e.g. relaxation time and heat capacity) can be regarded as temperature-independent during the simulation process. Hence, for a one-dimensional heat conduction system as shown in Fig. 1(b), we can set the total emission energy as $E = \Delta T \sum_p \int_0^{\omega_{\max,p}} v_g(\omega) C_\omega / 4 d\omega$. In this way, only the hot isothermal boundary needs to emit hot phonon bundles, and the cold isothermal boundary merely serves as an absorbing boundary. The net heat flow is then calculated by counting the number of phonon bundles arriving at the cold isothermal boundary.

As we stated above, the trajectories of phonon bundles are simulated independently, resulting in the significant computational merit when compared to the ensemble MC simulation. However, since the absorbing boundary is necessary for phonon tracing termination, periodic boundary condition that will lead to the absence of absorbing boundary, becomes inapplicable in the standard phonon tracing MC simulation. Therefore, when we use the standard phonon tracing MC method to calculate the effective thermal conductivity of a large area periodic nanostructure, the isothermal boundary conditions should be employed to establish the temperature difference. As shown in Fig. 1(b), the hot phonon bundles enter the computational domain from the hot isothermal boundary, and the specular boundary condition can be used as the alternative of the lateral periodic boundary condition [39]. We denote the number of the phonon bundles that arrive at the cold boundary by N_c, and then the net heat flux is calculated as

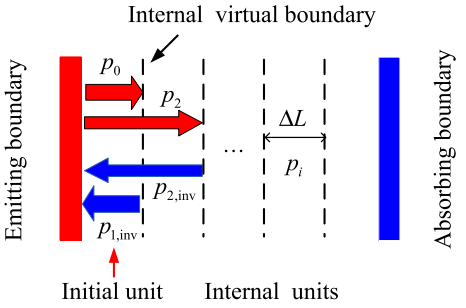

Fig. 3. Schematic for one-dimensional phonon transport system: p_0 is the initial phonon transmittance, and p_i is the internal phonon transmittance.

$$q = W N_c = p_t E, \tag{4}$$

where $p_t = N_c/N$ is the total phonon transmittance. Then, the effective thermal conductivity is given by

$$k_{\mathrm{eff}} = \frac{qL}{\Delta T} = p_t \frac{EL}{\Delta T}. \tag{5}$$

When $L \to \infty$, the end effect is completely eliminated, and thus we obtain the exact effective thermal conductivity of the large area periodic structure in theory. Obviously, $L \to \infty$ cannot be realized in practice, and thus a reliable way to obtain the exact effective thermal conductivity is to gradually increase the number of periods until the result is converged, which can cause large computational expense.

3. Algorithm of two-step MC method

A large area periodic nanostructure is comprised of a series of units whose length is denoted by ΔL, and thus can be regarded as a one-dimensional phonon transport system shown in Fig. 3. As long as we know the phonon transmittance of each simulation unit, the total phonon transmittance can be obtained. The initial simulation unit is directly in contact with the phonon emission boundary (i.e. hot isothermal boundary), and its phonon transmittance is denoted by p_0. Due to the periodicity of structure, it could be reasonable to assume that the internal units that are not directly in contact with the phonon emission boundary hold the same phonon transmittance p_i. The total phonon transmittance can be derived from p_0 and p_i. We assume the periodic nanostructure contains N_p units, and a recurrence relation is then derived,

$$\begin{aligned}
&N_p = 1, \quad p_1 = p_0;\\
&N_p = 2, \quad p_2 = p_1 p_i \sum_{j=1}^{\infty} \left[(1 - p_{1,\mathrm{inv}})(1 - p_i)\right]^{j-1} = \frac{p_1 p_i}{1 - (1 - p_{1,\mathrm{inv}})(1 - p_i)};\\
&\quad\vdots\\
&N_p = N_p, \quad p_{N_p} = p_{N_p-1} p_i \sum_{j=1}^{\infty} \left[(1 - p_{N_p-1,\mathrm{inv}})(1 - p_i)\right]^{j-1} = \frac{p_{N_p-1} p_i}{1 - (1 - p_{N_p-1,\mathrm{inv}})(1 - p_i)};
\end{aligned} \tag{6}$$

in which $p_{1,\mathrm{inv}} \cdots p_{N_p-1,\mathrm{inv}}$ are the inverse transmittances describing the possibility that phonons return to the emitting boundary from the internal virtual boundaries. The recurrence relation of the inverse transmittance can be given by

$$\begin{aligned}
&N_p = 1, \quad p_{1,\mathrm{inv}} = p_i;\\
&N_p = 2, \quad p_{2,\mathrm{inv}} = p_{1,\mathrm{inv}} p_i \sum_{j=1}^{\infty} \left[(1 - p_{1,\mathrm{inv}})(1 - p_i)\right]^{j-1} = \frac{p_{1,\mathrm{inv}} p_i}{1 - (1 - p_{1,\mathrm{inv}})(1 - p_i)};\\
&\quad\vdots\\
&N_p = N_p, \quad p_{N_p,\mathrm{inv}} = p_{N_p-1,\mathrm{inv}} p_i \sum_{j=1}^{\infty} \left[(1 - p_{N_p-1,\mathrm{inv}})(1 - p_i)\right]^{j-1} = \frac{p_{N_p-1,\mathrm{inv}} p_i}{1 - (1 - p_{N_p-1,\mathrm{inv}})(1 - p_i)}.
\end{aligned} \tag{7}$$

Thus, according to the recurrence relation, Eq. (7), the inverse transmittance of a nanostructure with N_p periods is

$$p_{N_p,\mathrm{inv}} = \frac{p_i}{1 + (N_p - 1)(1 - p_i)}. \tag{8}$$

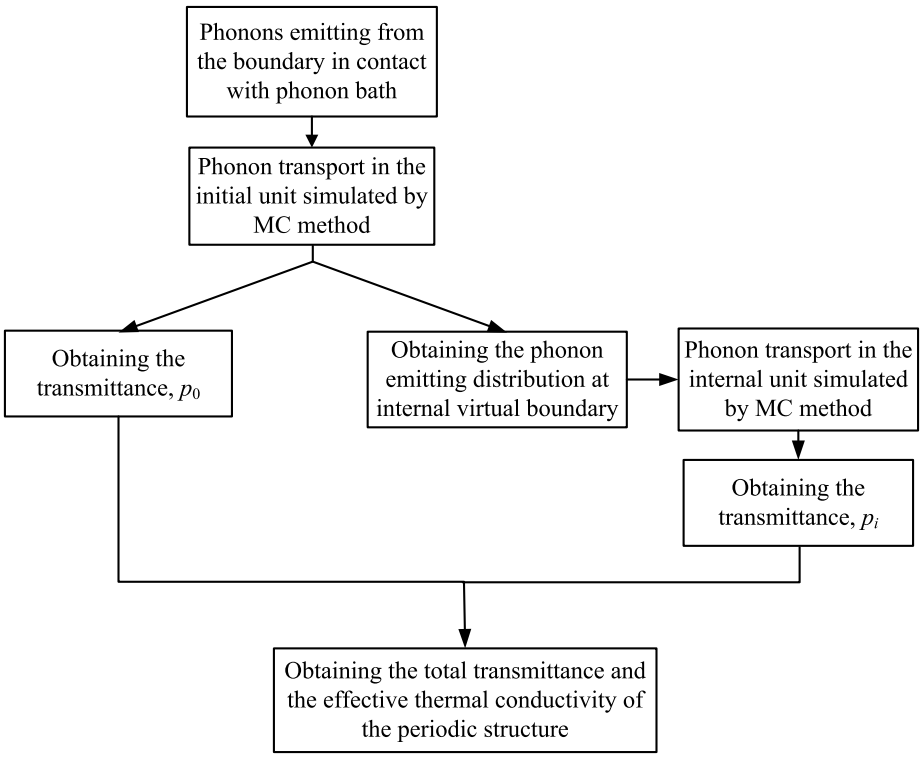

Fig. 4. Algorithm schematic for two-step Monte Carlo method.

Furthermore, combining Eqs. (6) and (8), we have the total phonon transmittance when a nanostructure contains N_p periods,

$$p_{N_p} = \frac{p_0}{1 + (N_p - 1)(1 - p_i)}. \tag{9}$$

In terms of Eq. (5), the effective thermal conductivity is then obtained,

$$k_{\text{eff},N_p} = p_{N_p} \frac{EL}{\Delta T} = \frac{E\Delta L}{\Delta T} \frac{p_0 N_p}{1 + (N_p - 1)(1 - p_i)}. \tag{10}$$

As $N_p \to \infty$ (i.e. $L \to \infty$), we have the limit effective thermal conductivity,

$$k_{\text{eff\_limit}} = \frac{E\Delta L}{\Delta T} \frac{p_0}{1 - p_i}. \tag{11}$$

Since the end effect is completely eliminated for the limit effective thermal conductivity, it can be regarded as an estimation of the exact effective thermal conductivity of the large area periodic nanostructure.

When the structure of the simulation unit is given, once we know how the phonon bundles enter the simulation unit, i.e. the boundary phonon emission distributions, its phonon transmittance can be calculated by using the phonon tracing MC method. The initial unit is in contact with the hot isothermal boundary where the phonon emission distributions are already known [13], so its transmittance, p_0, can be readily obtained by the standard phonon tracing MC simulation. In contrast, how the phonon bundles enter the internal unit (i.e. the phonon emission distributions at the internal virtual boundary) should be obtained by simulating the phonon transport in the initial unit. As shown in Fig. 3, the right absorbing boundary in the initial unit just serves as the phonon emission boundary for the internal unit, which means how the phonon bundles leave the initial unit determines how the phonon bundles enters the internal unit. Therefore, the phonon emission distributions at the internal virtual boundary can be obtained by gathering the statistics of phonon angular, spatial and frequency distributions at the right absorbing boundary of the initial unit. Fig. 4 shows the algorithm of the two-step MC method, which is concluded as two basic simulation steps: (1) We simulate the phonon transport in the initial unit, and then obtain the initial phonon transmittance p_0 and the phonon emission distributions at the internal virtual boundary; (2) According to the phonon emission distributions at the internal virtual boundary, the phonon transport in the internal unit is simulated to obtain the internal phonon transmittance p_i. Once p_0 and p_i are both obtained, we can calculate the effective thermal conductivity of the whole structure by using Eqs. (10) and (11).

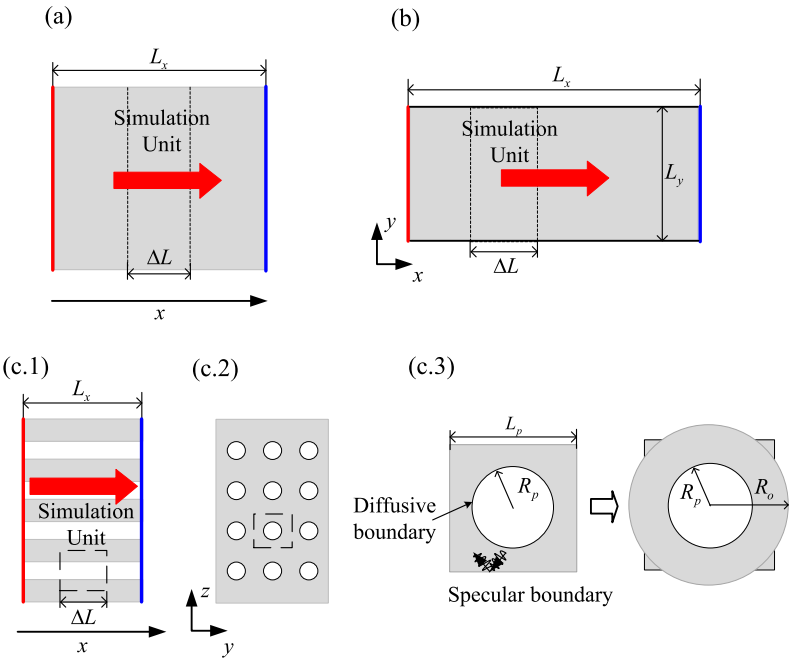

Fig. 5. (a) Schematic for cross-plane heat conduction in nanofilm; (b) Schematic for in-plane heat conduction in nanofilm; (c.1) Schematic for heat conduction in nanoporous structure; (c.2) Unit of nanoporous thin film: the outer surface can be approximated as a circle with the same area.

If the size of minimum repeating unit is much small, in order to reduce the estimation deviation of the two-step MC method, in practice one simulation unit can contain several minimum repeating units. Even in this way, the length of simulation unit, ΔL, can also be small (one MFP or even smaller), and thus the two-step MC method can gain a significant computational merit when compared to the standard phonon tracing MC simulation. Importantly, it does not require a complicated programming, because the structure of the initial and the internal simulation units is definitely the same, and what we need to do is just to renew the phonon emission distributions at the emitting boundaries. In addition, when the simulation unit length is larger than one MFP, the difference between p_0 and p_i resulted from the phonon boundary emission distributions is found to be negligible. Therefore, the two-step MC method can even be simplified as a one-step MC method, which can further reduce the computational expense, by taking p_0 as the alternative of p_i. Here, three main advantages of the two-step MC method can be concluded as below: (i) it can greatly reduce the computational expense without destroying the accuracy; (ii) it does not require a complicated programming; (iii) it can even be simplified a one-step MC method when the simulation unit length is considerably large.

4. Numerical experiments

We calculate the effective thermal conductivities of three typical silicon nanomaterials, i.e. cross-plane and in-plane nanofilms, and periodic nanoporous structures, as shown in Fig. 5, by using the theoretical models, the standard and the two-step phonon tracing MC simulations, respectively. These three nanostructures are relatively simple and thus hold reliable analytical effective thermal conductivity models derived from the phonon BTE, so they are good examples to verify the two-step MC method. For clarity, Debye approximation is adopted to deal with the phonon properties of silicon at the room temperature, and thus phonons travel with one average group velocity and the scattering rate is characterized by an average phonon MFP. Here, we choose the average MFP (l_0) as 260 nm with its corresponding heat capacity (0.93×10^6 J/m^3 K) and average group velocity (1800 m/s) [35]. Due to the Debye approximation, Eq. (10) can be simplified as

$$\frac{k_{\text{eff},N_p}}{k_{\text{bulk}}} = \frac{3\Delta L}{4l_0} \frac{p_0 N_p}{1 + (N_p - 1)(1 - p_i)}. \tag{12}$$

Then, Eq. (11) becomes

$$\frac{k_{\text{eff\_limit}}}{k_{\text{bulk}}} = \frac{3\Delta L}{4l_0} \frac{p_0}{1 - p_i}. \tag{13}$$

For silicon at room temperature, the dominant phonon wave length is approximately less than 1 nm [40], and thus any realistic surface roughness will lead to completely diffusive scattering at the boundaries. In our simulations, when phonons emit from the isothermal boundary, the angular emission distribution obeys Lambert's cosine law, and the spatial emission

Table 1
Phonon transmittances calculated by MC simulations.

	$\Delta L = 0.5$ MFPs		$\Delta L = 1$ MFP		$\Delta L = 5$ MFPs	
	p_0	p_i	p_0	p_i	p_0	p_i
Cross-plane	0.704	0.715	0.553	0.568	0.207	0.214
In-plane, $Kn_y = 1$	0.618	0.643	0.459	0.482	0.151	0.162
In-plane, $Kn_y = 5$	0.416	0.462	0.276	0.306	0.0772	0.0861
Nanoporous, $Kn_R = 1$, $\varepsilon = 0.2$	0.682	0.698	0.528	0.546	0.190	0.198
Nanoporous, $Kn_R = 5$, $\varepsilon = 0.1$	0.654	0.671	0.497	0.515	0.177	0.186

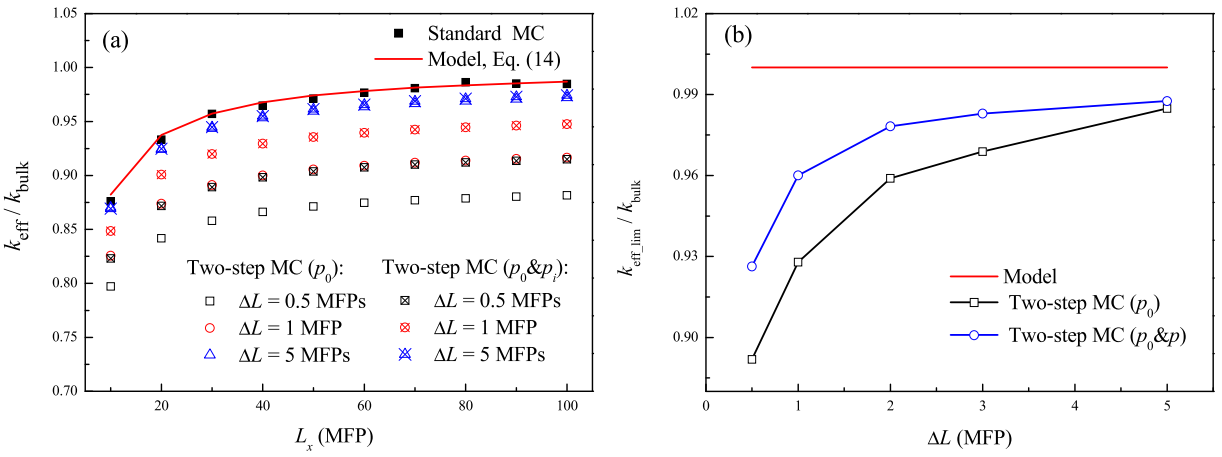

Fig. 6. (a) Cross-plane effective thermal conductivity varying with L_x; (b) Limit effective thermal conductivity of cross-plane nanofilm.

distribution is uniform at the boundaries. The internal scattering is set as isotropic. The number of phonon bundles that we trace in the simulations is set as 2×10^6. Besides, more information about the random number sampling can refer to Refs. [13,21].

4.1. Cross-plane heat conduction in nanofilm

Fig. 5(a) shows the cross-plane heat conduction in nanofilms. In this case, the film thickness is equal to the distance between phonon baths (L_x), and the effective thermal conductivity increases with the increasing film thickness, due to the influence of ballistic transport. On the basis of the differential approximate solution of the phonon BTE, the effective thermal conductivity of cross-plane nanofilms is given by [41]

$$\frac{k_{\text{eff,cr}}}{k_{\text{bulk}}} = \frac{1}{1 + \frac{4}{3}\frac{l_0}{L_x}}, \tag{14}$$

where k_{bulk} is the bulk thermal conductivity and l_0 is the average phonon MFP.

In the two-step MC simulations, the lengths of simulation unit (ΔL) are set as 0.5, 1 and 5 MFPs, respectively. As illustrated in Table 1, we calculate the initial and the internal phonon transmittances (p_0 and p_i) for the cross-plane nanofilms. The phonon transmittances reduce with the increasing L_x, and p_i is always larger than p_0. Then, the cross-plane effective thermal conductivities are obtained by using Eq. (12). Fig. 6(a) illustrates the cross-plane effective thermal conductivity of nanofilms varying with L_x. It found that the cross-plane effective thermal conductivity increases with increasing L_x, and the results obtained by the standard MC simulation agree well with these predicted by the theoretical model, Eq. (14). The results predicted by the two-step MC method are slightly less than these obtained by the standard MC method, and the deviation between them decreases with increasing length of simulation unit ΔL. As we stated above, the difference between p_0 and p_i could be small in some cases, and thus we can only use p_0 to estimate the effective thermal conductivity. The effective thermal conductivities obtained by the two-step MC method with using p_0 are less than these with using both p_0 and p_i, while their difference decreases with increasing ΔL. In the case with $\Delta L = 5$ MFPs, their differences can even be neglected. We may conclude that as $\Delta L \geq 5$ MFPs, the two-step MC method can be simplified as a one-step MC method by taking p_0 as the alternative of p_i, which will further reduce the computational cost.

In theory, as the distance between two phonon baths approaches to infinite, i.e. $L_x \to \infty$, the cross-plane effective thermal conductivity will recover to the bulk value, that is, $k_{\text{eff,cr}}/k_{\text{bulk}} = 1$. For the two-step MC method, using Eq. (13), we can estimate the limit effective thermal conductivity with $L_x \to \infty$ (i.e. $N_p \to \infty$). As shown in Fig. 6(b), the limit effective thermal conductivities predicted by the two-step MC method are slightly less than the bulk value, and their deviation

Table 2
Limit effective thermal conductivity of cross-plane nanofilm with $L_x \to \infty$.

	$k_{\text{eff\_limit}}/k_{\text{bulk}}$	$(k_{\text{bulk}} - k_{\text{eff\_limit}})/k_{\text{bulk}}$ (%)	Computation time (s)
Theoretical model, Eq. (14)	1.00	0	N/A
Standard MC, $L_x = 100$ MFPs	0.985	1.5%	29.4 (100%)
Two-step MC $\Delta L = 0.5$ MFPs	0.926	7.4%	0.841 (2.8%)
$\Delta L = 1$ MFP	0.958	4.2%	1.08 (3.6%)
$\Delta L = 5$ MFPs	0.988	1.2%	3.84 (13.1%)

Table 3
Limit effective thermal conductivity of in-plane nanofilms with $L_x \to \infty$.

		$k_{\text{eff\_limit}}/k_{\text{bulk}}$	$(k_{\text{bulk}} - k_{\text{eff\_limit}})/k_{\text{bulk}}$ (%)	Computation time (s)
$Kn_y = 1$	Theoretical model, Eq. (15)	0.684	0	N/A
	Standard MC, $L_x = 100$ MFPs	0.681	0.5%	80.5 (100%)
	Two-step MC $\Delta L = 0.5$ MFPs	0.651	4.8%	1.53 (1.9%)
	$\Delta L = 1$ MFP	0.664	2.9%	2.56 (3.2%)
	$\Delta L = 5$ MFPs	0.678	0.8%	8.83 (10.9%)
$Kn_y = 5$	Theoretical model, Eq. (15)	0.323	0	N/A
	Standard MC, $L_x = 100$ MFPs	0.315	2.5%	189 (100%)
	Two-step MC $\Delta L = 0.5$ MFPs	0.290	10.1%	2.79 (1.5%)
	$\Delta L = 1$ MFP	0.299	7.4%	4.74 (2.5%)
	$\Delta L = 5$ MFPs	0.316	2.2%	20.1 (10.6%)

decreases with increasing ΔL. Besides, we can also only use p_0 to predict the limit effective thermal conductivity. The results by the two-step MC method with using p_0 are less than these with using p_0 and p_i, and the difference also decreases with increasing ΔL. Although it cannot be realized in the standard MC simulation to let L_x approach to infinite, we can set L_x equal to 100 MFPs to approach to the limit effective thermal conductivity. As shown in Table 2, the deviation between the theoretical value and the result predicted by the standard MC simulation with $L_x = 100$ MFPs is about 1.5%. In contrast, for the two-step MC simulation, once $\Delta L \geq 1$ MFP, the deviation becomes less than 5%. More importantly, Table 2 demonstrates that the two-step MC method can greatly reduce the computation time without causing significant deviation. For example, as $\Delta L = 5$ MFPs, the deviation of the two-step MC simulation is only about 1.2%, while its computation time is one order of magnitude less than that of the standard MC simulation with $L_x = 100$ MFPs.

4.2. In-plane heat conduction in nanofilm

Fig. 5(b) shows the in-plane heat conduction in nanofilms. The in-plane effective thermal conductivity of nanofilms decreases due to the phonon-boundary scattering and merely depends on the lateral thickness L_y in theory [18],

$$\frac{k_{\text{eff\_in}}}{k_{\text{bulk}}} = 1 - \frac{3}{2}\frac{l_0}{L_y}\int_0^1 \left[1 - \exp\left(-\frac{l_0}{\sqrt{1-\mu^2}L_y}\right)\right]\mu^3 d\mu. \tag{15}$$

However, in practice, the distance between phonon baths, L_x, can also influence the in-plane effective thermal conductivity, unless $L_x \gg l_0$. Therefore, in the standard MC simulations, if we only want to investigate the L_y-dependence of effective thermal conductivity, the distance between phonon baths must be large enough to eliminate the end effect.

We define a Knudsen number as $Kn_y = l_0/L_y$. In our MC simulations, Kn_y is set as 1 and 5, respectively. Table 1 shows p_0 and p_i for the in-plane nanofilms with different lengths of simulation unit ($L_x = 0.5$, 1 and 5 MFPs). Due to the y-directional boundary scattering, the transmittances of in-plane films are less than these of cross-plane films, and decrease with Kn_y increasing. Figs. 7(a) and (b) illustrate the in-plane effective thermal conductivity of nanofilms varying with L_x. When Kn_y is given, the in-plane effective thermal conductivity increases with increasing L_x, and approaches to the value predicted by Eq. (15). The results predicted by the two-step MC method are slightly less than these obtained by the standard MC method, and the deviation between them decreases with increasing ΔL. Besides, the effective thermal conductivities obtained by the two-step MC method with using p_0 are less than these with using both p_0 and p_i, while the difference also decreases with increasing ΔL. Similar to the case of cross-plane nanofilms, when $\Delta L \geq 5$ MFPs, their difference can be neglected. Fig. 7(c) illustrates the limit effective thermal conductivity of in-plane nanofilms with $L_x \to \infty$. By using Eq. (13), we can obtain the limit effective thermal conductivities, which are slightly less than these predicted by Eq. (15). In spite of the different values of Kn_y, the deviation between the two-step MC simulation and the theoretical model decreases with increasing ΔL, and becomes less than 5% as $\Delta L \geq 1$ MFP (shown in Table 3). Similar to the case of cross-plane nanofilms, the results by the two-step MC method with using p_0 are also less than these with using both p_0 and p_i, and the difference decreases with increasing ΔL. Besides, according to Table 3, for the in-plane nanofilms, the two-step MC method can also greatly reduce the computational time without destroying the accuracy.

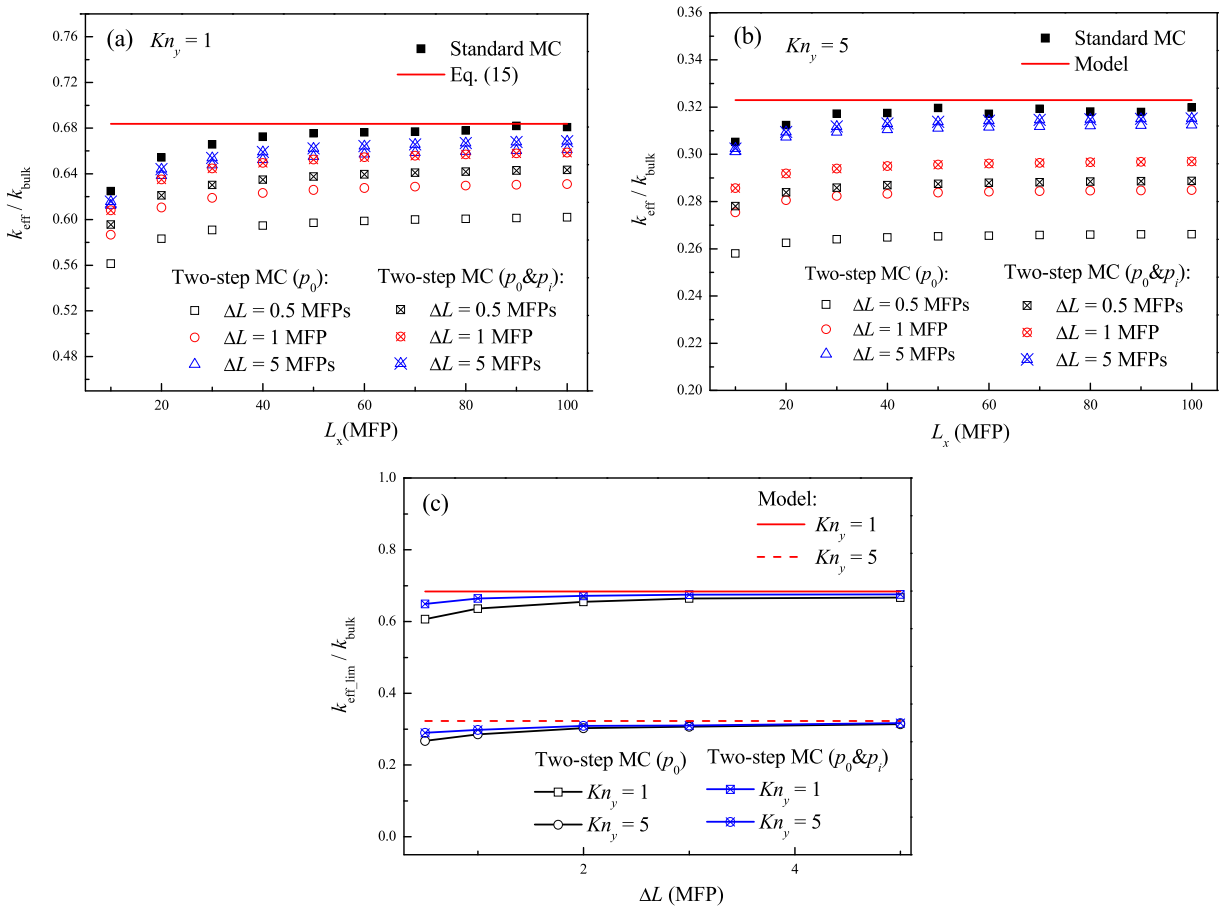

Fig. 7. (a) In-plane effective thermal conductivity with $Kn_y = 1$; (b) In-plane effective thermal conductivity with $Kn_y = 5$; (c) Limit effective thermal conductivity of in-plane nanofilm.

4.3. Heat conduction in periodic nanoporous structure

Figs. 5(c.1) and (c.2) show the heat conduction in a periodic nanoporous structure, which is crossed by nanoscale cylindrical channels. The pore radius is R_p, and the distance between two neighboring pore axials is L_p. The temperature difference is applied along the pore axial direction (x-direction), and thus the thermal transport is periodic in the y- and z-directions. Therefore, the phonon transport inside the nanoporous structures can be represented by that in the simulation unit shown in Fig. 5(c.3) with the totally specular scattering boundary conditions in the y- and z-boundaries [29]. It should be note that the specular scattering boundary conditions in the y- and z-boundaries do not change the transport direction of phonon energy, resulting in the same influence on effective thermal conductivity as that caused by the periodic boundary conditions. In our studying cases, pores are squarely arrayed, and thus the maximum porosity in theory is equal to $\pi/4 \approx 0.79$. For simplicity, the outer surface of the square unit is converted into a circle, that is, to approximate a square unit cross section as a circular cross section with the same cross-sectional area, as shown in Fig. 5(c.3), $R_o = L_p/\sqrt{\pi}$. And the porosity is then calculated as $\varepsilon = R_p^2/R_o^2$. According to above approximations, an analytical model for the effective thermal conductivity of host material along the pore axial direction can be derived from phonon BTE [24,40],

$$\frac{k_{\text{eff,po}}}{k_{\text{bulk}}} = 1 - \frac{3}{\pi R_p^2(\varepsilon^{-1}-1)} \int_{R_p}^{R_p/\sqrt{\varepsilon}} rdr \int_0^{2\pi} \int_0^1 \exp\left(-\frac{L_{rp}}{l_0\sqrt{1-\mu^2}}\right)\mu^2 d\mu d\varphi, \tag{16}$$

with

$$L_{rp} = \begin{cases} r\left[|\cos\varphi| - \left(\left(\frac{R_p}{r}\right)^2 - \sin^2\varphi\right)^{1/2}\right] & \pi - \varphi_{c1} \le \varphi \le \pi + \varphi_{c1} \\ \frac{R_p}{\sqrt{\varepsilon}}\frac{\sin(\varphi-\varphi_2)}{\sin(\varphi)} + \frac{R_p}{\sqrt{\varepsilon}}[|\cos\varphi_2| - (\varepsilon - \sin^2\varphi_2)^{1/2}] & 0 \le \varphi \le \varphi_{c1} \text{ or } 2\pi - \varphi_{c1} < \varphi \le 2\pi \end{cases}$$

in which $\varphi_{c1} = \arcsin(R_p/r)$ and $\varphi_2 = \arcsin[(r\sqrt{\varepsilon}/R_p)\sin(\varphi)]$.

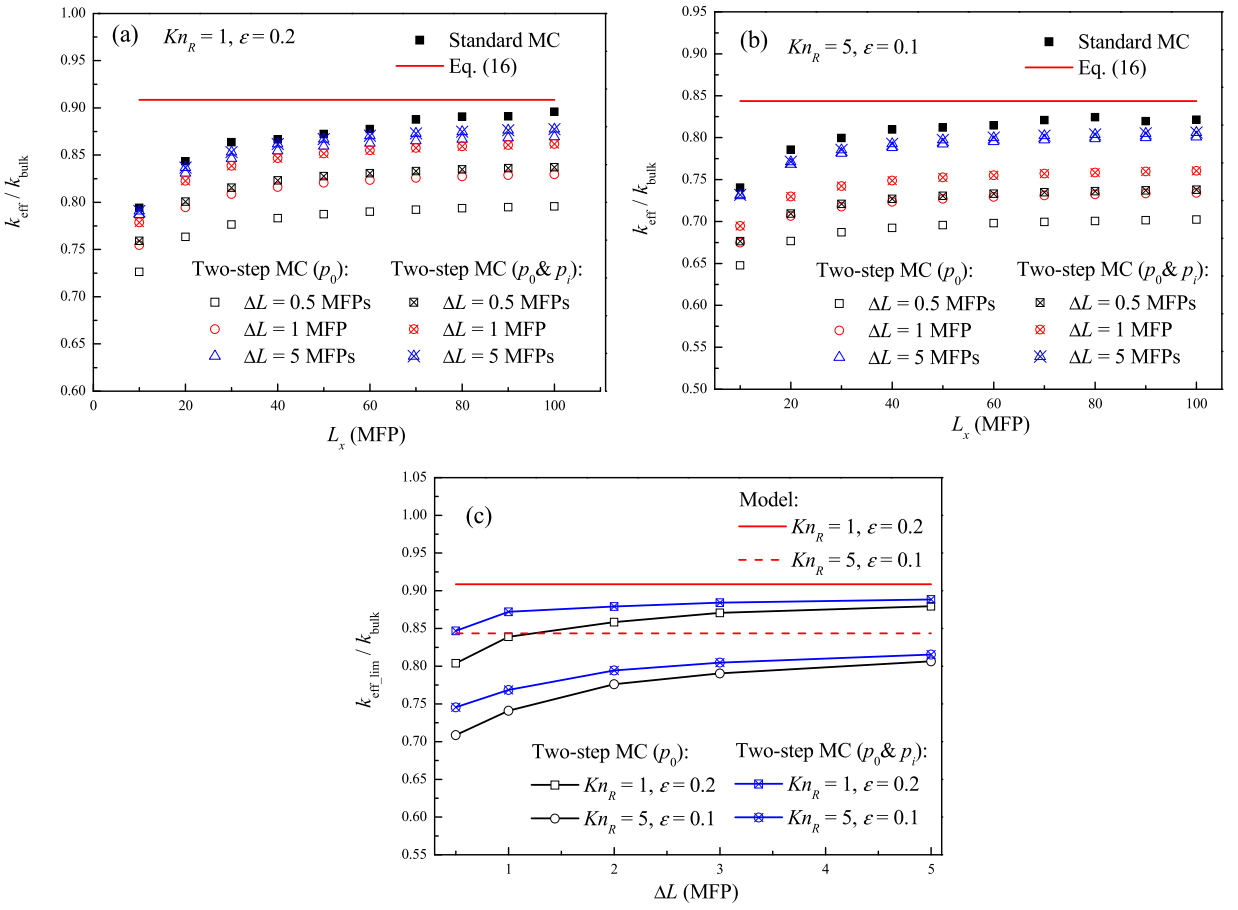

Fig. 8. (a) Effective thermal conductivity of nanoporous structure along the pore axial direction with $Kn_R = 1.0$ and $\varepsilon = 0.2$; (b) Effective thermal conductivity of nanoporous structure along the pore axial direction with $Kn_R = 5.0$ and $\varepsilon = 0.1$, (c) Limit effective thermal conductivity along the pore axial direction.

Table 4
Limit effective thermal conductivity of nanoporous structures with $L_x \to \infty$.

		k_{eff_limit}/k_{bulk}	$(k_{bulk} - k_{eff\_limit})/k_{bulk}$ (%)	Computation time (s)
$Kn_R = 1$, $\varepsilon = 0.2$	Theoretical model, Eq. (15)	0.908	0	N/A
	Standard MC, $L_x = 100$ MFPs	0.891	1.9%	103 (100%)
	Two-step MC $\Delta L = 0.5$ MFPs	0.846	6.8%	2.15 (2.1%)
	$\Delta L = 1$ MFP	0.871	4.1%	3.37 (3.3%)
	$\Delta L = 5$ MFPs	0.888	2.2%	10.9 (10.6%)
$Kn_R = 5$, $\varepsilon = 0.1$	Theoretical model, Eq. (15)	0.844	0	N/A
	Standard MC, $L_x = 100$ MFPs	0.831	1.5%	126 (100%)
	Two-step MC $\Delta L = 0.5$ MFPs	0.746	11.6%	2.63 (2.1%)
	$\Delta L = 1$ MFP	0.768	9.0%	3.88 (3.1%)
	$\Delta L = 5$ MFPs	0.816	3.3%	14.4 (11.4%)

The Knudsen number, Kn_R, is defined as $Kn_R = l_0/R$, and it is set as 1 and 5 respectively in the MC simulations. Table 1 also shows p_0 and p_i for nanoporous structure with different lengths of simulation unit ($\Delta L = 0.5$, 1 and 5 MFPs). Due to the pore boundary scattering, the transmittances of nanoporous structures are also less than these of cross-plane films. And when ε is given, the transmittances decrease with Kn_R increasing. Figs. 8(a) and (b) illustrate the effective thermal conductivity of this nanoporous structure along the pore axial direction varying with L_x. When Kn_R and ε are both given, the effective thermal conductivity of nanoporous structure increases with increasing L_x, and approaches to the value predicted by Eq. (16). Besides, Fig. 8(c) illustrates the limit effective thermal conductivity of nanoporous structure with $L_x \to \infty$, and Table 4 compares the computation times of the standard and the two-step MC simulations. We note that the same conclusions as these obtained in the cases of cross-plane and in-plane nanofilms can also be found for the nanoporous structures, which further verifies the validity and efficiency of our two-step MC method.

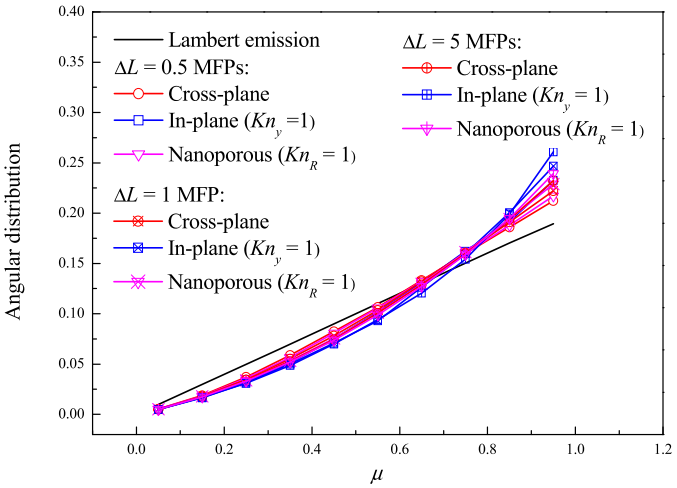

Fig. 9. Distributions of the cosine of polar angle of phonon boundary emission with various simulation unit lengths: $\mu = \cos\theta$.

4.4. Deviation analyses

According to these three numerical experiments above, we can conclude that the results predicted by the two-step MC method are slightly less than those obtained by the standard MC simulation, and their deviations can decrease with increasing lengths of simulation unit. For the two-step method, an important assumption has been adopted that the internal units hold the same phonon transmittance p_i, which should be responsible for this deviation. Actually, since the phonon boundary emission distributions at the internal virtual boundaries vary with increasing L_x, the phonon transmittances of internal units should also vary with increasing N_p, though their differences are considerably small especially for the cases with a large simulation unit length, as shown in Table 1.

Fig. 9 illustrates the distributions of the cosine of the polar angle ($\mu = \cos\theta$) of the boundary phonon emission with the various simulation unit lengths. We only take the polar angular distribution into account, since for angular distribution it is the dominant factor that influences the value of phonon transmittance in our numerical experiments. When phonon bundles emit from the isothermal boundary, Lambert's cosine law corresponds to the linear distribution of μ. Then, the internal and boundary scattering events in the simulation unit will make its distribution approach to parabola, which means the proportion of the phonon bundles whose μ is close to 1 increases when compared to Lambert's emission. For one given structure, the distribution of μ is shifted to the end of $\mu = 1$ with increasing ΔL, since more scattering events can influence the phonon transport in the unit with a larger length. This shift effect of angular distribution can lead to the increase of phonon transmittance of the internal units with increasing N_p. In Sec. 3, we neglect this effect and assume a same phonon transmittance of the internal units, which results in the under-prediction of the two-step MC method.

Fig. 10 shows the spatial distributions of boundary phonon emission with the various simulation unit lengths. When phonon bundles emit from the isothermal boundary, the spatial distribution should be uniform. Besides, the spatial distribution is always uniform in the cross-plane nanofilms due to the absence of the boundary scattering, and this is the reason why Fig. 10 does not illustrate the case of cross-plane nanofilm. As shown in Fig. 10, the diffusive boundary scattering in the simulation unit can reduce the number of emitting phonon bundles near the corresponding scattering boundaries, leading to the shift of spatial distribution to the region without the diffusive-scattering boundaries. As a result, the spatial distribution for in-plane nanofilm is shifted to the center region, while that for the nanoporous structure is shifted to the specular outer boundaries. The shift effect of spatial distribution can also cause the increase of the phonon transmittance. However, different from the angular distribution, the spatial distribution of phonon emission at the internal virtual boundary does not significantly vary with increasing ΔL, and thus only leads to the minor increase of the internal phonon transmittance with increasing N_p.

5. Conclusions

The phonon tracing MC simulation is an extensively-used method to simulate the phonon transport in nanostructures. However, due to the demand of absorbing boundaries, it cannot efficiently simulate the heat conduction in the large area periodic nanostructures yet. In the present work, we develop a two-step MC method to overcome the deficiency of the periodic boundary condition in the standard phonon tracing MC simulation. Our two-step MC method contains two basic simulation steps: (i) Phonon transport is simulated in the initial unit to obtain the initial phonon transmittance and the phonon emission distributions at the internal virtual boundary; (ii) According to the phonon emission distributions at the internal virtual boundary, the phonon transport in the internal unit is simulated to obtain the internal phonon transmittance.

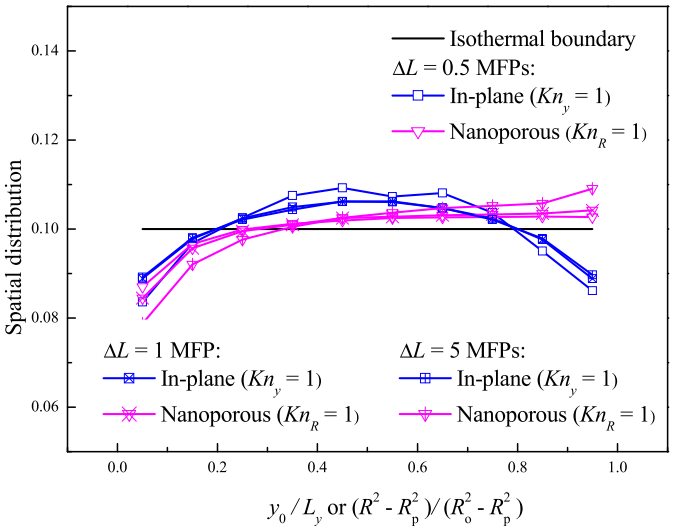

Fig. 10. Spatial distributions of phonon boundary emission with various simulation unit lengths.

By combining the initial and the internal phonon transmittances, we can derive the total phonon transmittance, and then obtain the effective thermal conductivity of the whole structure.

Three numerical experiments have been conducted to verify our two-step MC method. The two-step MC method well estimates the results by the standard MC simulation and the theoretical models. More importantly, it can greatly reduce the computation time without causing significant deviation, when compared to the standard MC method. As the length of simulation unit is larger than 1 MFP, the under-prediction of two-step MC method should be less than about 10% (even 5%), while the computation time is reduced by more than one order of magnitude. Besides, when the length of simulation unit is larger than 5 MFPs, the two-step MC method can even simplified as a one-step MC method by taking the initial phonon transmittance as the alternative of the internal phonon transmittance, which can further reduce the computation expense. In fact, our two-step MC method could also be extended to investigate the radiation transfer and the neutron transport problems such as modeling the ceramics nuclear fuels [42], since all these phenomena can be characterized by the Boltzmann transport equation.

Acknowledgements

This work is financially supported by National Natural Science Foundation of China (Nos. 51676108, 51356001), and Science Fund for Creative Research Groups (No. 51621062), the Tsinghua National Laboratory for Information Science and Technology of China (TNList).

References

[1] H. Alam, S. Ramakrishna, A review on the enhancement of figure of merit from bulk to nano-thermoelectric materials, Nano Energy 2 (2013) 190–212.
[2] G. Galli, D. Donadio, Thermoelectric materials: silicon stops heat in its tracks, Nat. Nanotechnol. 5 (2010) 701–702.
[3] J. Lim, H.T. Wang, J. Tang, et al., Simultaneous thermoelectric property measurement and incoherent phonon transport in holey silicon, ACS Nano 10 (2016) 124–132.
[4] J.K. Yu, S. Mitrovic, D. Tham, et al., Reduction of thermal conductivity in phononic nanomesh structures, Nat. Nanotechnol. 5 (2010) 718–721.
[5] F.X. Alvarez, D. Jou, A. Sellitto, Pore-size dependence of the thermal conductivity of porous silicon: a phonon hydrodynamic approach, Appl. Phys. Lett. 97 (2010) 033103.
[6] R. Anufriev, M. Nomura, Thermal conductance boost in phononic crystal nanostructures, Phys. Rev. B 91 (2015) 245417.
[7] J. Ziman, Electrons and Phonons, Oxford University Press, London, 1961.
[8] D.G. Cahill, P.V. Braun, G. Chen, et al., Nanoscale thermal transport. II. 2003–2012, Appl. Phys. Lett. 1 (2014) 011305.
[9] A.J. Minnich, Determining phonon mean free paths from observations of quasiballistic thermal transport, Phys. Rev. Lett. 109 (2012) 205901.
[10] A. Mittal, S. Mazumder, Hybrid discrete ordinates—spherical harmonics solution to the Boltzmann Transport Equation for phonons for non-equilibrium heat conduction, J. Comput. Phys. 230 (2011) 6977–7001.
[11] T. Klitsner, J.E. VanCleve, H.E. Fischer, R.O. Pohl, Phonon radiative heat transfer and surface scattering, Phys. Rev. B 38 (1988) 7576–7594.
[12] R.B. Peterson, Direct simulation of phonon-mediated heat transfer in a Debye crystal, J. Heat Transf. 116 (1994) 815–822.
[13] S. Mazumder, A. Majumdar, Monte Carlo study of phonon transport in solid thin films including dispersion and polarization, J. Heat Transf. 123 (2001) 749–759.
[14] Q. Hao, G. Chen, M.S. Jeng, Frequency-dependent Monte Carlo simulations of phonon transport in two-dimensional porous silicon with aligned pores, J. Appl. Phys. 106 (2009) 114321.
[15] V. Jean, S. Fumeron, K. Termentzidis, et al., Monte Carlo simulations of phonon transport in nanoporous silicon and germanium, J. Appl. Phys. 115 (2014) 024304.
[16] S. Wolf, N. Neophytou, H. Kosina, Thermal conductivity of silicon nanomeshes: effects of porosity and roughness, J. Appl. Phys. 115 (2014) 204306.

[17] M.S. Jeng, R.G. Yang, D. Song, G. Chen, Modeling the thermal conductivity and phonon transport in nanoparticle composites using Monte Carlo simulation, J. Heat Transf. 130 (2008) 042410.
[18] J.P.M. Péraud, N.G. Hadjiconstantinou, Efficient simulation of multidimensional phonon transport using energy-based variance-reduced Monte Carlo formulations, Phys. Rev. B 84 (2011) 205331.
[19] J.P.M. Péraud, N.G. Hadjiconstantinou, An alternative approach to efficient simulation of micro/nanoscale phonon transport, Appl. Phys. Lett. 101 (2012) 153114.
[20] J. Schleeh, J. Mateos, I. Íñiguez-de-la-Torre, et al., Phonon black-body radiation limit for heat dissipation in electronics, Nat. Mater. 14 (2015) 187–192.
[21] Y.C. Hua, B.Y. Cao, Phonon ballistic-diffusive heat conduction in silicon nanofilms by Monte Carlo simulations, Int. J. Heat Mass Transf. 78 (2014) 755–759.
[22] Y.C. Hua, B.Y. Cao, Ballistic-diffusive heat conduction in multiply-constrained nanostructures, Int. J. Therm. Sci. 101 (2016) 126–132.
[23] Y.C. Hua, B.Y. Cao, The effective thermal conductivity of ballistic-diffusive heat conduction in nanostructures with internal heat source, Int. J. Heat Mass Transf. 92 (2016) 995–1003.
[24] Y.C. Hua, B.Y. Cao, Cross-plane heat conduction in nanoporous silicon thin films by phonon Boltzmann transport equation and Monte Carlo simulations, Appl. Therm. Eng. 111 (2017) 1401–1408.
[25] Y.C. Hua, B.Y. Cao, Anisotropic heat conduction in two-dimensional periodic silicon nanoporous films, J. Phys. Chem. C 121 (2017) 5293–5301.
[26] N.K. Ravichandran, A.J. Minnich, Coherent and incoherent thermal transport in nanomeshes, Phys. Rev. B 89 (2014) 205432.
[27] J. Lee, W. Lee, G. Wehmeyer, et al., Investigation of phonon coherence and backscattering using silicon nanomeshes, Nat. Commun. 8 (2017) 14054.
[28] Y.C. Hua, B.Y. Cao, Transient in-plane thermal transport in nanofilms with internal heating, Proc. R. Soc. A 472 (2016) 20150811.
[29] D.S. Tang, Y.C. Hua, B.D. Nie, B.Y. Cao, Phonon wave propagation in ballistic-diffusive regime, J. Appl. Phys. 119 (2016) 124301.
[30] D.S. Tang, Y.C. Hua, B.Y. Cao, Thermal wave propagation through nanofilms in ballistic-diffusive regime by Monte Carlo simulations, Int. J. Therm. Sci. 109 (2016) 81–89.
[31] D.S. Tang, B.Y. Cao, Ballistic thermal wave propagation along nanowires modeled using phonon Monte Carlo simulations, Appl. Therm. Eng. 117 (2017) 609–616.
[32] B.Y. Cao, W.J. Yao, Z.Q. Ye, Networked nano-constrictions: an effective route to tuning the thermal transport properties of graphene, Carbon 96 (2016) 711–719.
[33] Y. Wang, B. Qiu, X. Ruan, Edge effect on thermal transport in graphene nanoribbons: a phonon localization mechanism beyond edge roughness scattering, Appl. Phys. Lett. 101 (2012) 013101.
[34] M. Nomura, Y. Kage, J. Nakagawa, et al., Impeded thermal transport in Si multiscale hierarchical architectures with phononic crystal nanostructures, Phys. Rev. B 91 (2015) 205422.
[35] G. Chen, Thermal conductivity and ballistic-phonon transport in the cross-plane direction of superlattices, Phys. Rev. B 57 (1998) 14958.
[36] A.J. Minnich, G. Chen, S. Mansoor, et al., Quasiballistic heat transfer studied using the frequency-dependent Boltzmann transport equation, Phys. Rev. B 84 (2011) 235207.
[37] K. Esfarjani, G. Chen, H.T. Stokes, Heat transport in silicon from first-principles calculations, Phys. Rev. B 84 (2011) 085204.
[38] D. Baillis, J. Randrianalisoa, Prediction of thermal conductivity of nanostructures: influence of phonon dispersion approximation, Int. J. Heat Mass Transf. 52 (2009) 2516–2527.
[39] R. Yang, G. Chen, M.S. Dresselhaus, Thermal conductivity of simple and tubular nanowire composites in the longitudinal direction, Phys. Rev. B 72 (2005) 125418.
[40] R. Prasher, Thermal conductivity of composites of aligned nanoscale and microscale wires and pores, J. Appl. Phys. 100 (2006) 034307.
[41] A. Majumdar, Microscale heat conduction in dielectric thin films, J. Heat Transf. 115 (1993) 7–16.
[42] M. Stan, Discovery and design of nuclear fuels, Mater. Today 12 (2009) 21–27.